

10/28/82

IMAGING AND CHARACTERIZATION OF DEFECTS WITH DIGITAL
SIGNAL PROCESSING OF ULTRASONIC DATA

B. A. Barna and J. A. Johnson
EG&G Idaho, Inc.
Idaho Falls, ID 83415

INTRODUCTION

This paper describes the continuation of the work^{1,2} on synthetic-aperture focusing techniques (SAFT) and ultrasonic imaging as well as new work on the measurement of the amplitude and phase as a function of frequency and aperture position.

The previous synthetic-aperture studies had demonstrated a new algorithm which included corrections for variations in the front surface of the part being inspected and removed distortions in the enhanced image due to these variations. In addition, flat transducers were used to produce enhanced images which were nearly equal in quality to the images produced using focused transducers.

In this work the algorithm is tested and extended to enhance images of a test sample with an extremely deformed surface (Section 2.1) and to enhance images produced using shear waves (Section 2.2).

Finally, a preliminary report of some new measurements of the amplitude and phase of the ultrasonic signal as a function of aperture position and frequency of the signals reflected from a crack is given in Section 3.

SYNTHETIC-APERTURE FOCUSING TECHNIQUES

The following sections present images for raw data and for two types of enhancement: SAFT processing without and with corrections for deviations of the surface from a horizontal

plane. Changes in the processing algorithm which were necessary to handle an extremely deformed surface (Section 2.1) and the shear-wave data (Section 2.2) are discussed. Problems and recommendations are discussed in Section 2.3.

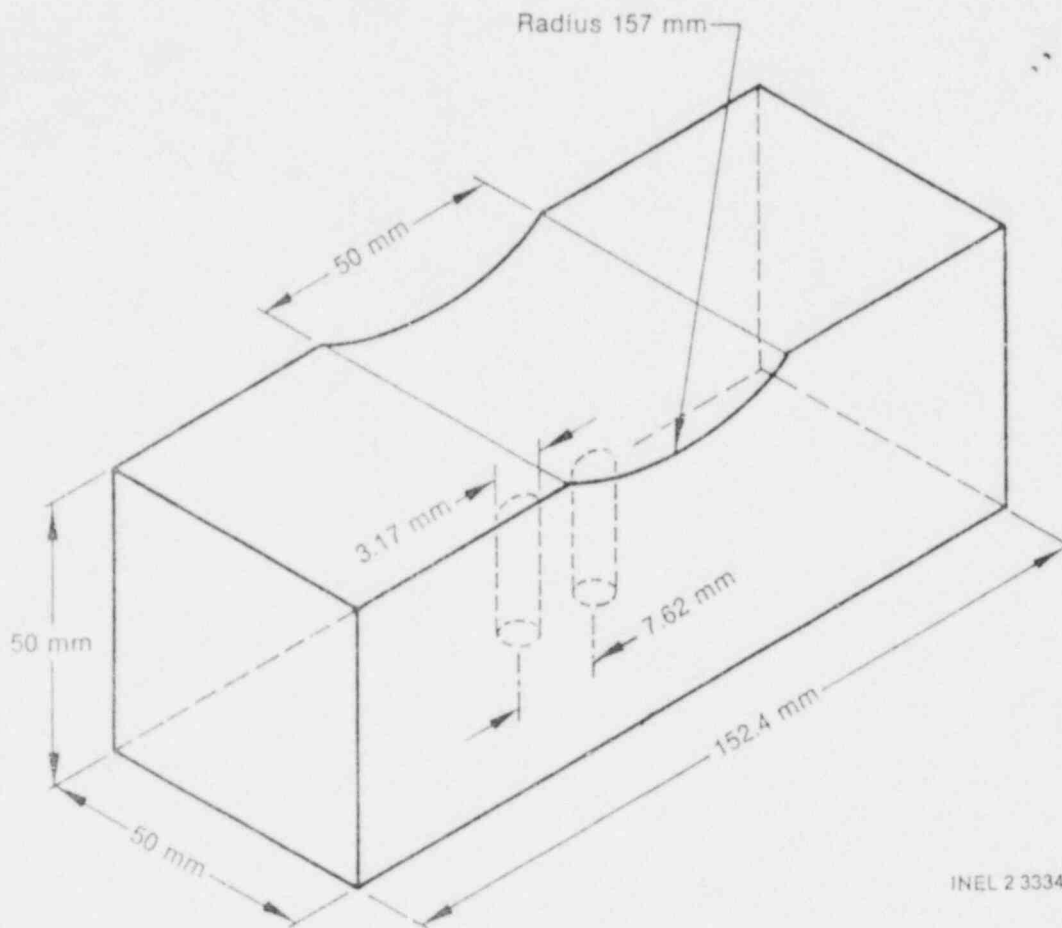
Data is taken using the automated ultrasonic testing (AUT) system which is described in more detail in Reference 2. For the longitudinal scans (Section 2.1) a test sample of aluminum is placed in a laboratory scanning tank and the transducer is moved over the block under computer control. The 2.25 MHz, 12.5 mm-diameter, flat transducer is adjusted to be normal to the flat portion of the surface and is scanned along a line parallel to the long dimension of the block (x direction) at a sample period of 1.0 mm. The sample period along the A-scan direction is 50 ns which corresponds to 0.158 mm in the metal. Three line scans are made: one directly over the center line of the round-bottom hole or holes and one 1.0 mm on each side. Only data from the center scan is used to produce the images given in this paper. The shear-wave data is acquired in the same manner except that the transducer is tilted at a 19.6° angle from the normal to produce a 45° shear wave in the metal block (for a flat, horizontal surface). The sample rate along the A-scan direction is still 50 ns, but this corresponds to 0.0782 mm in the metal for the slower shear wave.

The images are produced on a DICOMED D48 COM unit. Each plot is a representation of the sonic echoes received from the blocks, which contain one or two round-bottom holes. The B-scan plots have the x axis parallel to the scan line and the z axis perpendicular the scan line and positive into the block. Each A scan is filtered after processing to obtain a video envelope. The longitudinal data in Section 2.1 are interpolated in the x direction to obtain square pixels of 0.16 mm on a side. The shear-wave data of Section 2.2 are averaged in the A-scan direction to obtain square pixels of 1.0 mm on a side. The shear-wave images are produced using the reconstruction program PLOTTER which is the main analysis tool in the AUT system.

Effect of Extreme Surface Distortion

A test block used for the images in this section is shown in Fig. 1. The block has had a concave area machined off the surface directly above two round-bottom holes with the dimensions shown in the figure.

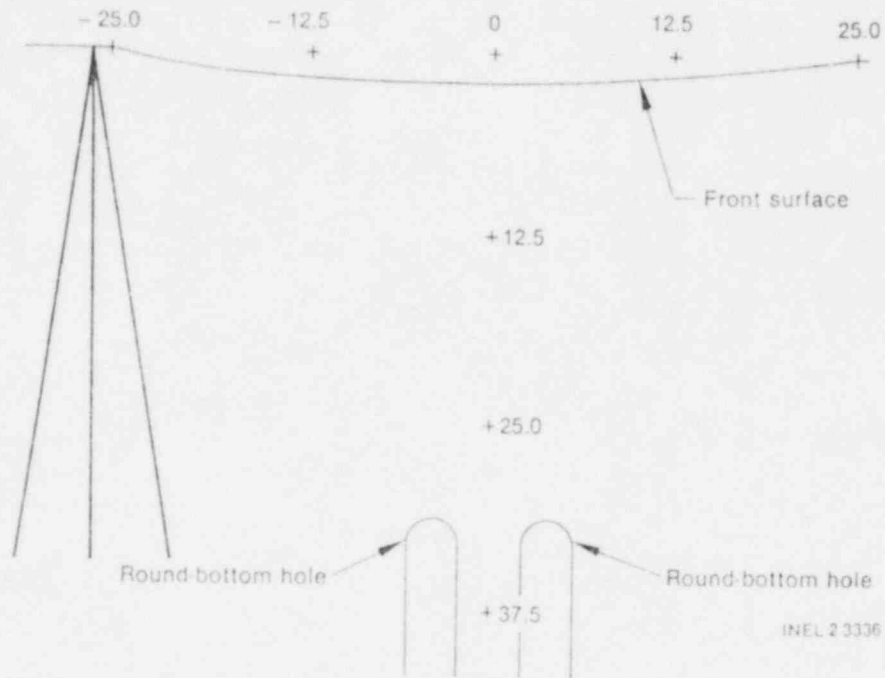
The slope of the front surface changes abruptly from zero degrees to nine degrees at the edge of the machined area. This relatively large slope, coupled with the large sound-speed ratio causes the refracted rays to change direction dramatically as the transducer is moved over the block. Figure 2a shows the sound-



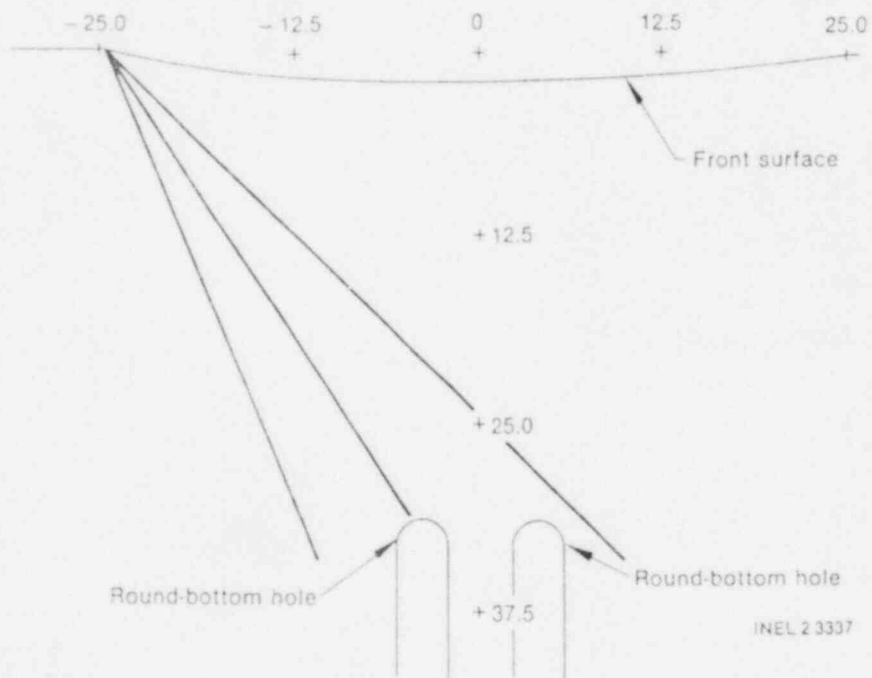
INEL 2 3334

Fig. 1. Test Block SN4. A concave area of width 50.0 mm and radius of curvature 157 mm is milled out of the center of the flat front surface. Two round-bottom holes of diameter 3.18 mm with center-to-center distance of 7.62 mm are at the center of the block in line with the long dimension.

beam pattern at zero slope, assuming the beam spread is eight degrees in metal at normal incidence. At the edge of the machined areas the beam does not intersect the holes. However, when the transducer is moved to the right just far enough to see the nine-degree slope, the refracted beam is centered on the left target as shown in Fig. 2b. When the transducer is halfway to the center of the machined area as shown in Fig. 2c, the central beam is still on the left target. Figure 2d shows the refracted beam when the transducer is at the center of the machined area.

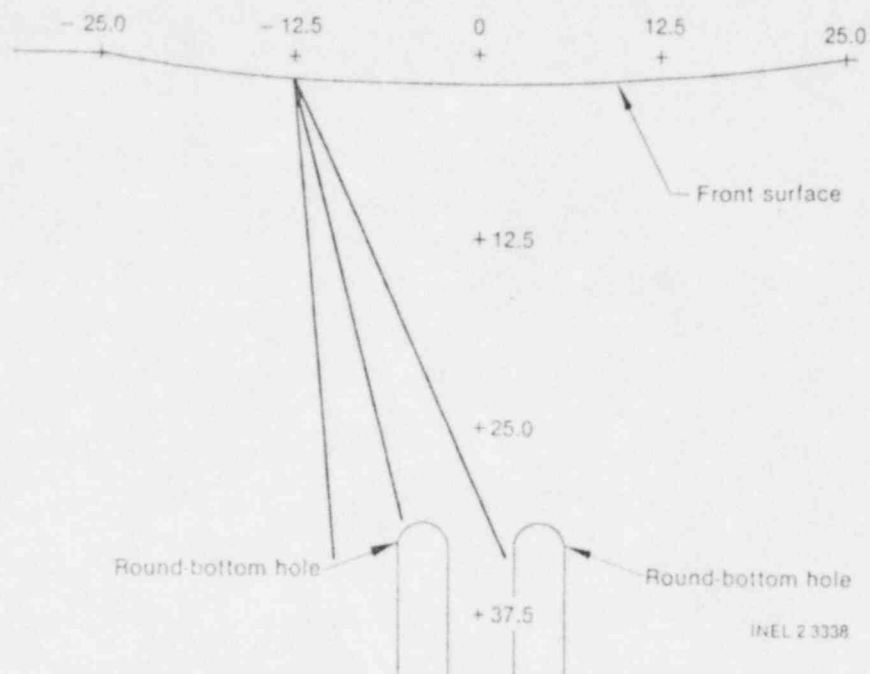


a. Transducer over flat portion of the surface.

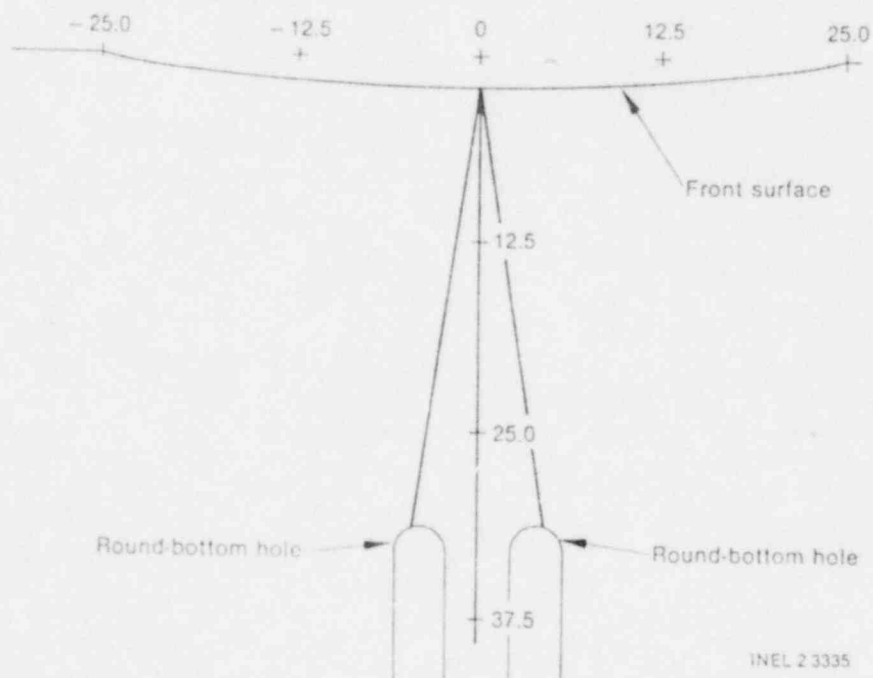


b. Transducer over the beginning of the concave area of the surface.

Fig. 2. Assumed beam pattern for various transducer positions.



- c. Transducer halfway to the center of the concave area of the surface.



- d. Transducer at the center of the concave area of the surface.



Fig. 3. Directed-beam B-scan image of a target block (SN4) with a concave surface and two round-bottom holes spaced 7.62 mm on center. The horizontal direction is parallel to the transducer scan line and the vertical direction is into the target block.

The B-scan image produced by this unprocessed data is shown in Fig. 3. The imaging program assumes a flat surface so the information in each A scan is placed in pixels directly below the transducer position. Since the transducer sees the holes at the edge of the machined area, the pixels below that point show a large indication. The net result is that the hole indications are 19.9 mm in width (3 dB). This is more than double the 3-dB width of an image of an identical single round-bottom hole in a sample with flat surface. In addition, the spacing between the centers of the hole images is 20.52 mm compared to the actual spacing of 7.6 mm.

Enhancing the image using SAFT without correcting for surface variations results in little improvement, as shown in Fig. 4. The processing assumes that the transducer can see a target point only



Fig. 4. Analytic surface SAFT-processed B-scan image of the data shown in Fig. 3. The processing assumes a flat, horizontal front surface and does not correct for the refraction effects of the true concave surface.

over a limited range of transducer positions determined by the refraction angles of the beam assuming a flat surface. Actually, we see from Fig. 2b that the beam at the left edge of the machined area has information about the hole on the right. However, this A scan is not included in the correlated A scan for an equivalent transducer position directly over the right-hand hole. The changing water path over the scan path also distorts the processing. The distance in water is magnified by more than a factor of four due to the sound speed ratio of metal to water. The center A scan has an extra 2.0 mm of water which the flat-surface processing algorithm assumes is metal of thickness 8.5 mm. Thus, there is a large error of over 65° of phase in the correlation process over an aperture containing the machined area.

In attempting to account for the surface deviations, several difficulties are encountered. In previous work the front surface echo was used to locate the surface for the processing algorithm.³ Since the front surface signal saturated the electronics, the first saturated value was used to find the surface. For this extreme surface, however, this technique does not work since the transducer side-lobe signals can sometimes produce the first saturation, resulting in discontinuities in the obtained surface coordinates. The side-lobe reflection off the sloping surface does return a significant amount of energy to the transducer and the interference of the side-lobe signal with the main-lobe signal changes the position of the saturated value in a complex way which cannot easily be related to the distance to the surface. This problem is even worse for the transverse scans where the side-lobe signal arrives before the main-lobe reflection and reflects from a position on the surface which is relatively far from the centerline of the transducer.

The front-surface detection routine is therefore modified to identify the front surface at that point in the A scan where the signal is just a few counts above noise. This results in an improved but not perfect reproduction of the actual surface. The actual surface and the surface obtained using this method are shown in Fig. 5. The reflections from the front surface from the edge of the central beam are received sooner than those from along the center line of the transducer when the transducer is over the machined area, resulting in an apparently closer surface. This results in a steeper slope and larger angles of refraction for the transmitted rays. For example, the measured slope at a point directly over the left hole was 5.3° while the actual slope at that point was only 1.4° . The result of this is that the ray-tracing algorithm using the larger slope does not find a ray in the central beam which intersected the left hole. Thus this position is not included in the correlated A scan for that hole.

The original processing algorithm assumes that the aperture is composed of a contiguous set of A scans. The diagrams in Fig. 2 show that to focus at some points, the aperture must be made up of two or more sets of contiguous A scans. For example to focus at the right-hand hole we would include A scans from transducer positions from the left edge of the machined area (Fig. 2b) to about $x = -15$ mm. We see in Fig. 2c that A scans from about here to a point just to the left of $x = 0$ do not contain information about the right-hand hole. These should be left out of the aperture. The A scans from this hole to the right edge of the machined area do include information about this hole and should be included in the aperture. The algorithm has been modified to account for this type of split aperture.

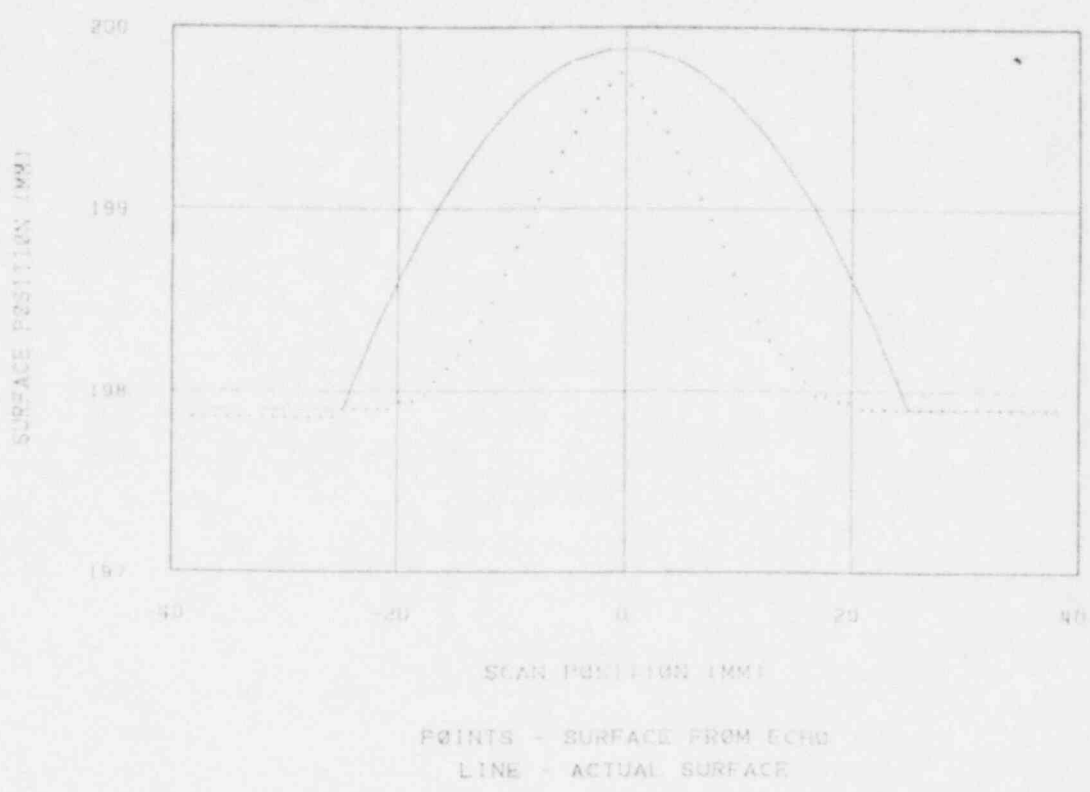


Fig. 5. The actual surface of target SN4 (line) shown with the surface derived from the first echo of the sound beam (points). Note that increasing surface position is into the target block making the surface concave.

Figure 6 shows the image obtained using the experimentally-derived surface pictured in Fig. 5. We see that the holes are well resolved in spite of the errors in the surface coordinates. However, although improved over the images in Figs. 3 and 4, this image has lateral position errors due to the front surface inaccuracies.

When the correct surface coordinates are used in the processing, the image in Fig. 7 is produced. This image demonstrates that, given the correct surface coordinates, the processing algorithm will produce an accurate image. The actual positions of the holes are very close to the image positions and the 3-dB width is less than that for a flat surface. This decreased width is due to the increased aperture. In Figs. 2a-d, we see that the holes can be seen over most of the machined area, which is more than double the distance they can be seen with a flat surface.



Fig. 6. Data for sample 224 with front-surface-correcting SAFT routine using the surface derived from the front surface echo shown in Fig. 5. The images of the round-bottom holes have improved resolution. The holes are mislocated by 1.88 mm and 0.86 mm.

Table 1 presents a summary of the data in this section. The first line gives the actual dimensions of the block. The succeeding lines give the information derived from images of: raw data; SAFT-processed using an assumed flat surface; SAFT-processed using the surface coordinates derived from the front surface echoes; and SAFT-processed using the actual surface coordinates. The last line, included for comparison, is for SAFT processed data from a block with identical holes but with a flat horizontal surface. This data is from Fig. 19 in a previous report.⁴ All the data are in millimetres and the widths are the 3-dB widths.

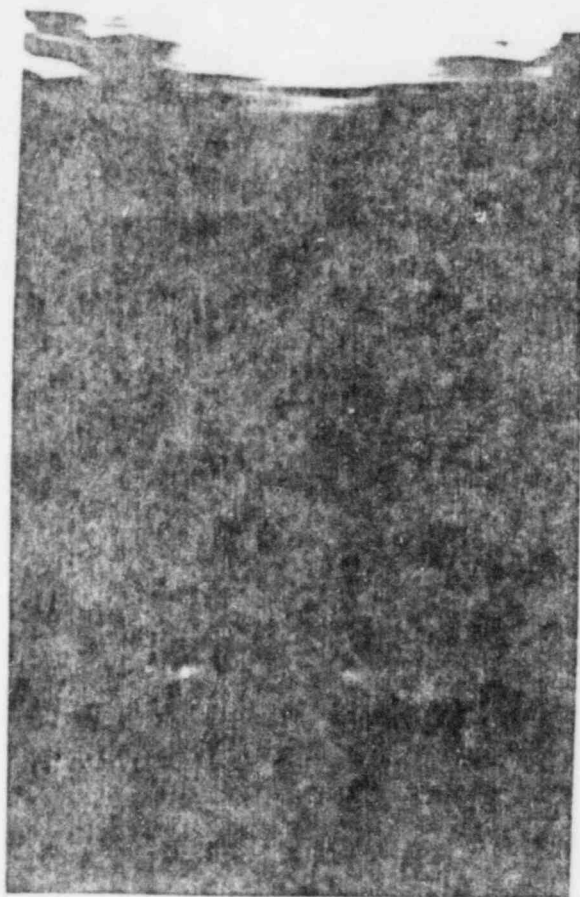


Fig. 7. Data for sample SN4 with front-surface-correcting SAFT routine using the true surface coordinates. These images of the holes are properly located.

SAFT With Shear Waves

Inspection using shear waves has advantages over that using longitudinal waves in many cases. The shear wavelength is usually about half that of longitudinal waves, resulting in better resolution. Front-surface ringdown, caused by a large front-surface reflection, is not a problem with the angled beam used to produce shear waves. This section discusses the application of SAFT to shear wave data without and with corrections for variations in the surface.

Three aluminum test blocks are imaged using shear waves. The first (SN1) has a single round-bottom hole at a depth of 31.75 mm with a diameter of 3.175 mm. The second (SN2) has two round-bottom holes with a center-to-center separation of 6.10 mm. The

TABLE 1. Data from Block with Surface Distortion

| Data | Width | Positions (mm) | | | | Lateral Separation (mm) |
|-----------------|-------|-------------------|-------|-------|-------|-------------------------------|
| | | x | z | x | z | |
| Block SN4 | 3.18 | -3.81 | 31.75 | 3.81 | 31.75 | 7.62 |
| Raw data | 19.94 | -9.83 | 36.83 | 10.70 | 36.83 | 20.52 |
| Flat surface | 11.58 | -8.89 | 37.34 | 10.33 | 37.34 | 19.25 |
| Derived surface | 3.44 | -5.69 | 30.48 | 4.67 | 30.48 | 10.36 |
| True surface | 2.05 | -3.81 | 32.80 | 3.86 | 32.80 | 7.67 |
| BRE10A | 6.16 | -3.63 | 33.27 | 3.63 | 33.27 | 7.26 |

third (SN6) has two round-bottom holes with a center-to-center separation of 7.62 mm. Blocks SN1 and SN2 have flat, horizontal front surfaces. Block SN6 has a machined surface that slopes at 3.6° . All three blocks have been imaged previously using longitudinal waves.⁵

The same flat transducer used for experiments discussed in the previous section is used for the shear wave work. It is tilted at an angle of 19.6° with respect to the vertical, resulting in a transmitted shear wave at 45° in the metal for a flat, horizontal surface. The scan is in the direction of the tilt angle, parallel to the long dimension of the block (x direction). Three line scans are made, but only data from the center scan directly above the center of the hole or holes is used to create the images.

The AUT analysis program PLOTTER is used to reconstruct and plot the images. The reconstruction process traces each A scan through a rectangular space of pixels and places each digitized value of the A scans in the nearest pixel. An assumption in the reconstruction process leads to errors in the positions of the images: the beginning of each A scan is at the surface of the part being inspected, which is assumed to be a plane parallel to the scan plane of the transducer. This surface is taken to be the origin of the depth (z) coordinate. Following this assumption, the program calculates the path of the A scan using the refracted angle and the speed of sound in the part being imaged. When the

A-scan data begins in the water outside the part, as is the case in all the data sets in this report, the data is incorrectly placed in the pixels for two reasons: the distance between the digitized data values in water is from one-half to one-fourth the distance assumed by PLOTTER using the metal sound speed (this distance is thus magnified by a factor of two to four); secondly, the actual angle of the A-scan data at the beginning is the incident angle, but the program assumes it is the refracted angle for the entire A scan.

For longitudinal scans only the first error is important, since the incident and refracted angles are the same. This is true even with a sloping surface, since the SAFT algorithm calculates an equivalent A scan which has a 0° incident and refracted angle by choosing the synthetic focus to match that geometry. The first error is partially corrected by using the surface coordinates to remove the appropriate number of points at the beginning of the A scan so that the data points in the water are replaced by an equivalent number assuming the metal sound speed. The net result is that the origin of the depth coordinate is some known distance above the surface of the part rather than at the surface. However since the surface clearly shows in the image, the depth positions of the flaws may be easily measured relative to that surface. The reconstruction introduces no error in the lateral position in the case of longitudinal scans.

Both sources of error are important for shear waves. The first error is again partially compensated by changing the number of data points at the beginning of the A scan to replace the water path by an equivalent metal path. However, the incorrect angle can produce an error in both the lateral and depth position. Further, an error in locating the surface can result in additional errors in image position since the water path correction would be in error. The image of the surface is poor or nonexistent in these correlated scans since the reflections are weak and not in focus, thus removing a reference from which to measure in the image.

Table 2 presents the results of the data derived from the images of Blocks SN1 and SN2. Since both these blocks have flat, horizontal front surfaces, no surface processing is required. Figures 8 and 9 show the images for unprocessed and processed data for target SN1. Figures 10 and 11 show the images for SN2.

The large errors in the positions of the hole images for the unprocessed data are due to the two errors in the reconstruction program discussed above. These errors are larger than those that would normally be observed in directed beam images since the normal procedure is to set up the data acquisition system so that the data in each A scan does begin at the position of the assumed

TABLE 2. Shear Wave Data from Block with Flat Surface

| Data | Width (mm) | Positions (mm) | | | | Lateral Separation (mm) |
|--------------|---------------|-------------------|-------|-------|-------|-------------------------------|
| | | x | z | x | z | |
| Block SN1 | 3.18 | 0.0 | 31.75 | | | |
| Raw data | 4.57 | 9.32 | 42.55 | | | |
| Flat surface | 2.40 | 6.86 | 40.39 | | | |
| Block SN2 | 3.18 | -3.05 | 31.75 | 3.05 | 31.75 | 6.10 |
| Raw data | 5.36 | 8.36 | 41.91 | 13.41 | 42.42 | 5.05 |
| Flat surface | 2.79 | 4.83 | 40.39 | 10.80 | 40.39 | 5.97 |

flat, horizontal front surface. In this case, however, in order to determine if the front surface could be accurately mapped using the ultrasound echo, the acquisition system is set so that there is some data in each A scan before the front surface.

The processed images are improved in two respects:

1. The resolution is improved by nearly a factor of two in both cases. The actual resolution is probably better than indicated since the actual width of the hole is larger than the -3-dB width of the image. However, the 45° shear wave only reflects from a portion of the round-bottom hole.
2. The position errors in the hole image are decreased. Part of the remaining position error is due to the reconstruction, but part is also due to a slight mislocation of the assumed surface of about 5.5 mm that is used in the ray tracing to the synthetic focus in the processing algorithm.

Table 3 presents the data for Block SN6 with the sloping surface. Here the unprocessed image (Fig. 12) has the same errors mentioned above plus an error due to the sloping surface. The reconstruction program assumes a flat, horizontal surface and calculates a refraction angle of 45°. The actual refraction angle is about 30° when the sloping surface is taken into

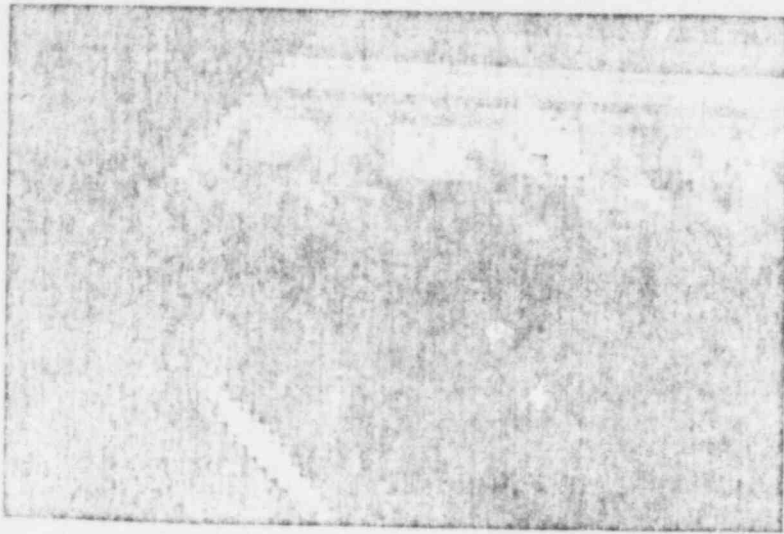


Fig. 8. Directed-beam, reconstructed B-scan image of a target SN1 using shear waves at 45°. This target has a flat, horizontal front surface and a single round-bottom hole.



Fig 9. Analytic surface SAFT-processed, reconstructed B-scan image of the data in Fig. 8. The hole is misplaced in lateral position and in depth due to error in locating the position of the front surface.



Fig. 10. Directed-beam, reconstructed B-scan image of target SN2 using shear waves at 45° . This target has a flat, horizontal front surface and two round-bottom holes with center spacing of 6.10 mm.



Fig. 11. Analytic surface SAFT-processed, reconstructed B-scan image of the data in Fig. 10. Again the holes are misplaced due to an error in the assumed surface location.

TABLE 3. Shear Wave Data from Block with Sloping Surface

| Data | Width (mm) | Positions (mm) | | | | Lateral Separation (mm) |
|-----------------|---------------|-------------------|-------|-------|-------|-------------------------------|
| | | x | z | x | z | |
| Block SN6 | 3.18 | -3.81 | 31.75 | 3.81 | 31.75 | 7.62 |
| Raw data | 5.16 | 10.16 | 45.47 | 17.27 | 43.18 | 7.11 |
| Flat surface | 2.59 | 8.56 | 41.40 | 16.05 | 40.39 | 7.49 |
| Derived surface | 2.51 | -1.19 | 40.64 | 6.35 | 40.64 | 7.54 |

account. The processed image (Fig. 13) obtained assuming a flat, horizontal surface shows similar position errors but also exhibits improved resolution.

The surface-corrected SAFT processed image (Fig. 14) has even further improvements in resolution and a significant decrease in position errors. The resolution improvement is due to the different apertures used to calculate the correlated A scans. The improved aperture calculation is made possible by the surface mapping. The decrease in position error is also due to the surface mapping. Each synthetic focal point is chosen so that it will be on the line of a ray that is assumed to refract at the angle that the reconstruction program assumes, 45° . However, errors are still present which are due to the changing water path, and these change with transducer position.

The front surface location is determined by the first echo in the A scan that is a few counts above the noise level. However, the transducer side-lobe signal is the first signal received by the transducer. The distance to the front surface calculated from the time to the first echo. The signal is assumed to come from the surface directly below the transducer. This assumption, that the side-lobe signal comes from a point directly below the transducer, is used since it is found that this signal disappears when the transducer is moved past the edge of the block. Using this assumption, the calculated surface coordinates along the center of the beam differ by 0.8 mm in the lateral direction and 5.2 mm in range (z direction) from those found by assuming the echo comes from a point along the centerline of the transducer.



Fig. 12. Directed-beam, reconstructed B-scan image of target SN6 using shear waves at 45° . This target has a front surface which has a 3.6° slope and two round-bottom holes with center spacing 7.62 mm.



Fig. 13. Analytic surface SAFT-processed, reconstructed B-scan image of the data in Fig. 14. The resolution is improved but the images of the holes are not properly located.



Fig. 14. Shear-wave data for target SN6 processed with front-surface-correcting SAFT. The images are still misplaced but by less than those in Fig. 13. The error is due to a mislocation of the surface as shown in Figs. 15a and 15b and due to the reconstruction process which assumes that the entire A scan is in metal at the shear-wave angle. Because of the varying water path with the varying surface, different portions of the A scans are actually in water at the incident angle, causing a variable error in the location of each A scan.

In summary, we have completed a study of SAFT processing using shear waves. A substantial improvement in resolution is obtained with the processing. However, the goal of reducing position errors is only partially met because of two problems: first, some assumptions inherent in the reconstruction program PLOTTER are not compatible with data sets with variable surfaces; and second, the side lobes of the transducer produce echoes that come before the echo from the centerline of the beam in some geometries, thus distorting the derived surface coordinates. This is similar to the problem encountered in applying surface mapping to the concave machined surface in the L-wave studies.

Problems and Recommendations

The Surface-Mapping-SAFT program is successful in producing images using longitudinal and shear waves in samples with flat, sloped, and curved surfaces. In this process a number of problems have been uncovered and a number of new ideas have been tried with varying success. The initial emphasis of accounting for variable surfaces in the processing in order to obtain more accurate flaw positions, is only the first step in obtaining improved images.

Further work needs to be done to improve the reconstruction process and to account for other effects such as anisotropy and variable sound speeds.

The basic SAFT algorithm is successful in producing correlated A scans which, given the correct surface coordinates, result in improved resolution and decreased position errors, for both longitudinal and transverse data. The two major difficulties encountered in this work are related to obtaining correct surface coordinates and in actually reproducing the reconstructed B scan image from the correlated A scans. For the first problem, either further study is required to account for and use the side-lobe reflections from the front surface or some other method, such as a mechanical feeler, must be used to obtain accurate surface coordinates. One group has reported some success in masking the side lobes and this may be a useful technique.⁶ The second problem is well understood but will require a major rewrite of the reconstruction program PLOTTER.

PHASE AND FREQUENCY MEASUREMENTS

The surface-mapping image reconstruction techniques developed were next applied to a series of surface breaking cracks in a stainless steel bars. Since the sonic echos from these cracks are primarily specular, the SAFT processing did little to improve the image. Three different sized cracks were imaged and the only obvious distinguishing feature was signal amplitude, which is widely regarded as a less-than-ideal discriminator for flaw size.

Since much of the work conducted in this program showed that subtle effects in the phase and frequency of the signals across an aperture appear to be related to flaw size and configuration, the data collected from the cracks was reanalyzed with respect to these variables. The objective was to determine if there was non-amplitude, non-imaging information indicative of crack depth.

The cracks were examined with ultrasound refracted at a 45° angle in the material. A schematic of the data collection process is shown in Fig. 15. Ultrasonic echoes from the specular reflection from the root of the cracks were digitized and recorded at a variety of positions across a viewing aperture. The very small signal from the tip of the crack was not included in the analysis. However, the phase measurement of the signals in this case is complicated by the fact that at each new transducer position a large phase shift occurs due to a difference in signal transit time caused by the tilt of the transducer face with respect to the flat part surface. It is possible to remove this effect (essentially, this is a transducer field correction) and again plot the phase shift versus the position in the aperture.

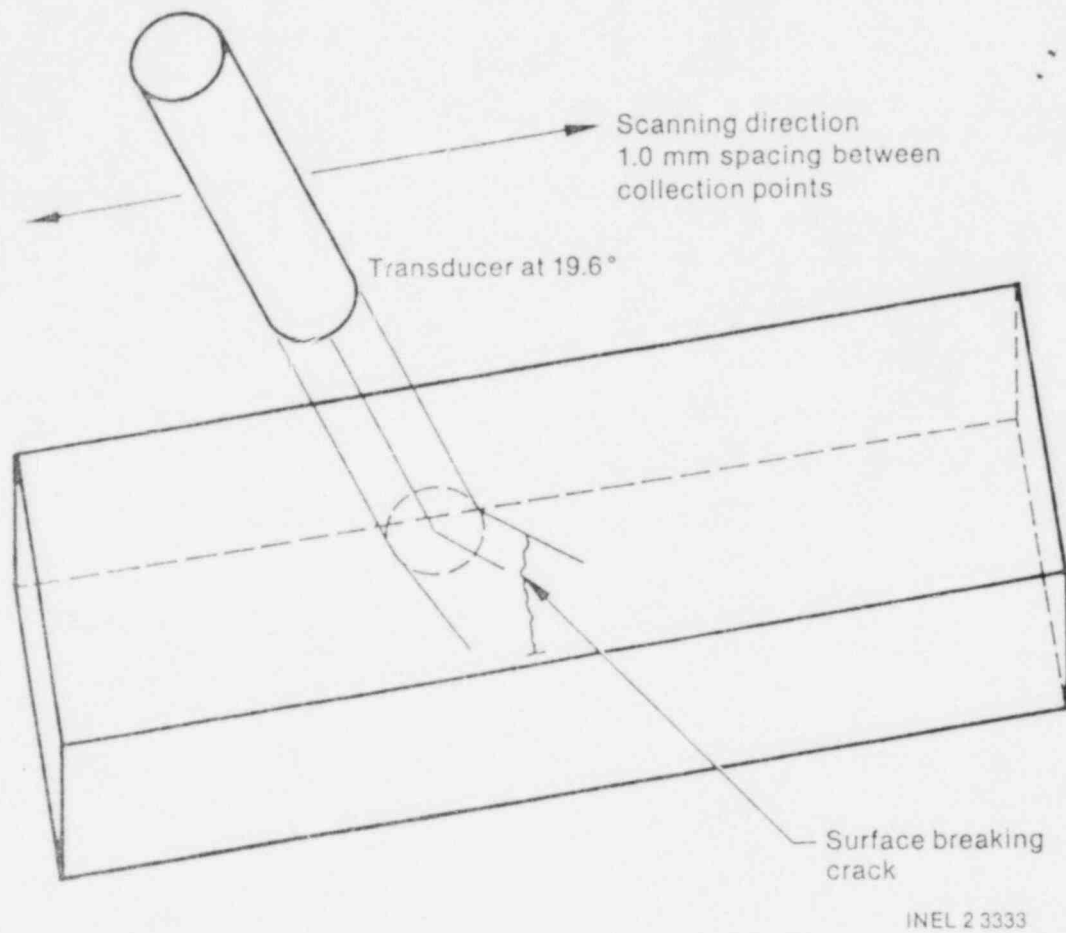


Fig. 15. Experimental setup for measuring phase of echo from a crack.

The amount of phase shift varies over the aperture according to the size of the crack (see Fig. 16). Note that the effect is not well defined on one side of the aperture but appears to be quite regular on the other; i.e., smaller cracks show larger shifts. A better understanding of the reasons for these differences may result in a predictive model that could provide a new method for sizing or characterizing cracks.

The crack samples not only showed effects in the phase measurements but also showed significant differences in amplitude spectra measurements across the aperture. Figure 17 shows plots of the ratio of two frequency components (1.25 and 3.44 MHz) across the aperture for the three different sized reflectors. A variation that follows the size of the crack is again evident and demonstrates the potential value of using both the amplitude and phase spectra of the signals to gain more information.

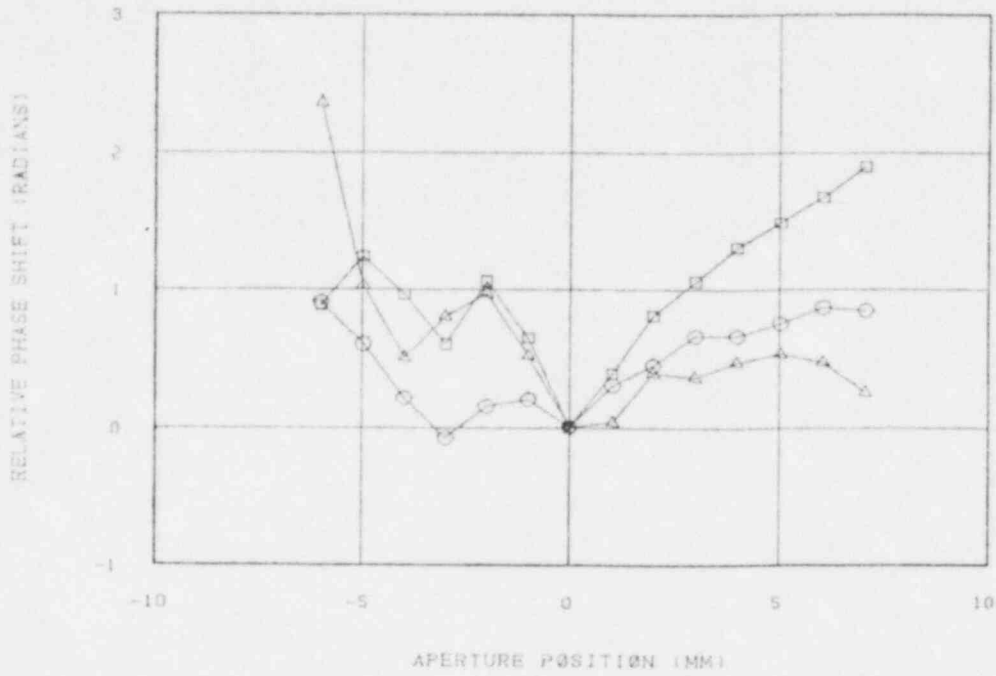


Fig. 16. Phase shift at 1.25 MHz for 1.5 (square), 3.0 (circle), 6.1 (triangle) mm cracks.

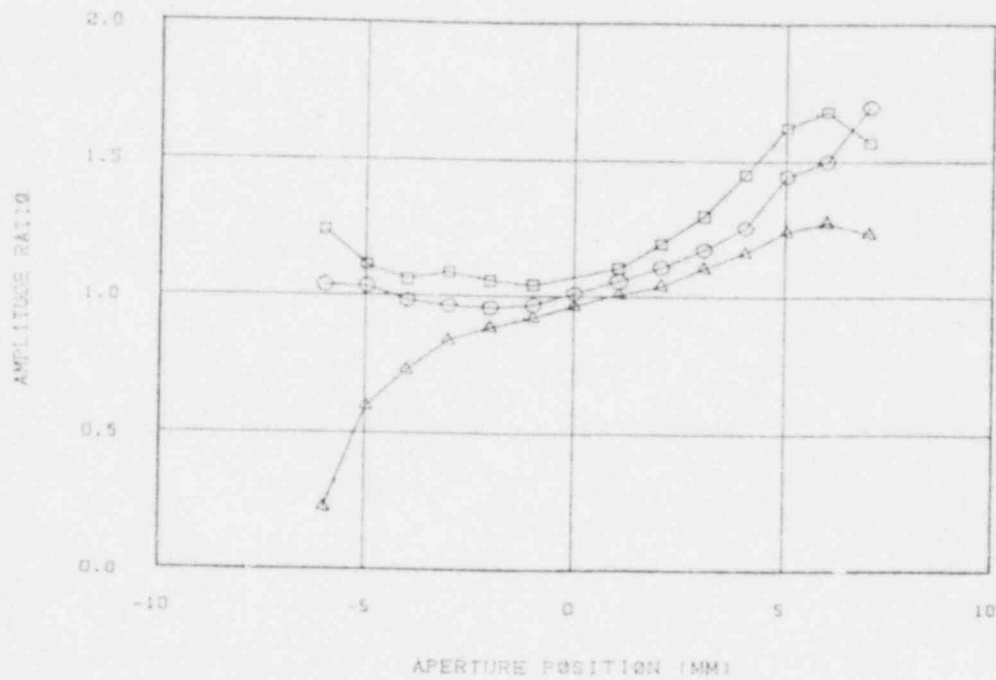


Fig. 17. Amplitude ratio at 1.25 and 3.44 MHz for 1.5 (square), 3.0 (circle), and 6.1 (triangle) mm cracks.

These differences in the spectra across the aperture for various sized cracks are more pronounced when the analysis is performed at lower ultrasonic frequencies. This lends credence to the postulate that the modification to the received signal caused by the reflector shape and size is primarily due to diffractive effects.

While these simple experiments do not take into account complicating factors such as mechanical scanning accuracy and effects of material velocity variations on phase measurements, they do show conclusively that residual effects occur which are solely due to the reflector modification of the field. Further, the complicated deconvolution problem is avoided by finding the transducer effects analytically and by keeping the analysis in the frequency domain. A more complete understanding of these phenomena through both experiments and theoretical models can provide a new method for characterizing objects with acoustic energy.

ACKNOWLEDGMENTS

This work was supported by the U.S. Department of Energy Assistant Secretary for Energy Research, Office of Basic Energy Sciences, under DOE Contract No. DE-AC07-76ID01570.

REFERENCES

1. B. A. Barna and J. A. Johnson, "The Effects of Surface Mapping Corrections with Synthetic-Aperture Focusing Techniques on Ultrasonic Imaging," Review of Progress in Quantitative Nondestructive Evaluation, Boulder, Colorado, August 3-7, 1981, to be published.
2. B. A. Barna and J. A. Johnson, "The Effects of Surface Mapping Corrections with Synthetic-Aperture Focusing Techniques on Ultrasonic Imaging," EGG-FM-5314, January 1981.
3. Ibid, p. 15.
4. Ibid, p. 37.
5. Ibid, p. 12.
6. J. L. Jackson, "Program for Field Validation of the Synthetic Aperture Focusing Technique for Ultrasonic Testing," NUREG/CR-1885, January 1981, pp. 31-33.